Determining the Strength of the Deep Western Boundary Current Using the Chlorofluoromethane Ratio*

ROBERT S. PICKART AND NELSON G. HOGG

Woods Hole Oceanographic Institution, Woods Hole, Massachusetts

WILLIAM M. SMETHIE, JR.

Lamont-Doherty Geological Observatory, Columbia University, Palisades, New York

(Manuscript received 1 August 1988, in final form 23 January 1989)

ABSTRACT

The dilution of a passive tracer during deep water formation and the subsequent advection/mixing in a deep boundary current is modeled with application to chlorofluoromethanes (CFMs) in the North Atlantic. Two different types of boundary currents are considered: a uniform flow and a simple shear flow. In each case the core of the flow mixes with surrounding water, which continually accumulates CFMs. In an extreme case the coupled system predicts that the CFM ratio in the current is unaltered from the ratio of its source water (save for a time lag). More realistic cases however suggest that the ratio is not a conserved quantity, but is substantially altered in both the overflow basin and boundary current. Matching the model results to CFM data collected near the Grand Banks gives a predicted (average) core speed of 5–10 cm s^{-1} for the Deep Western Boundary Current, and provides a constraint on the transport and diffusivity of the flow as well.

1. Introduction

Manmade chlorofluoromethanes (CFMs) enter the surface waters of the ocean by gas exchange, and as a result of convection at high latitudes are introduced at abyssal depths in the North Atlantic Ocean via the deep overflows. Large concentrations of the CFMs F-11 (CCl_3F) and F-12 (CCl_2F_2) have been detected at several locations in the deep western boundary current (DWBC) (for example, Gammon and Bullister 1982; Smethie and Trumbore 1984; Fine and Molanari 1988), and in warmer southward flowing water along the western boundary (Weiss et al. 1985).

CFMs are especially appealing as passive tracers because they are characterized by a high signal to noise ratio (Hogg et al. 1986), can be measured aboard ship, and their source function is well known. F-11 and F-12 concentrations in the troposphere are known from measurements since the mid-1970s (Rasmussen et al. 1981; Cunnold et al. 1983a; Cunnold et al. 1983b; Cunnold et al. 1986). Prior to this, F-11 and F-12 concentrations in the atmosphere can be determined from industrial release data (McCarthy et al. 1977; Chemical Manufacturers Association 1983) and the atmospheric lifetimes of F-11 and F-12 (Cunnold et al. 1986). Smethie et al. (1988) discuss this procedure in detail.

The atmospheric concentration of F-11 has until recently increased in time at a faster rate than that of F-12. This has led to the application of deducing the strength of subsurface boundary currents, particularly the deep western boundary current (DWBC) and flow of warmer water from the Labrador Sea. It is assumed that while the F-11 and F-12 content in a deep boundary current will be diluted due to mixing, their relative amount will remain constant, i.e. the F-11:F-12 ratio will be conserved since the interior deep basins are nearly void of CFMs. This means that a F-11:F-12 ratio measurement obtained downstream can be matched to the ratio of the source water to determine when the water parcel was isolated from the sea surface, thus giving the speed of the current. This argument assumes the ratio is unaltered during the deep-water formation and overflow process.

CFM dating has been applied to the DWBC by Smethie and Trumbore (1984) to differentiate between the source waters of the current. Weiss et al. (1985) applied it to the TTO dataset and deduced a 1–2 cm s^{-1} flow of water along the western boundary originating from the Labrador Sea. In the past several years the F-11:F-12 ratio curve has flattened out, even decreasing for a short period (Fig. 1). A measured ratio which is near the level of this plateau can at best determine the age of the water within a range of several years, an ambiguity which was present in both of the above studies.

In summer of 1983, cruise OC134 crossed the

* Lamont-Doherty Geological Observatory Contribution Number 4463.

Corresponding author address: Dr. Robert S. Pickart, The University of Rhode Island, Graduate School of Oceanography, Narragansett Bay Campus, Narragansett, RI 02882-1197.

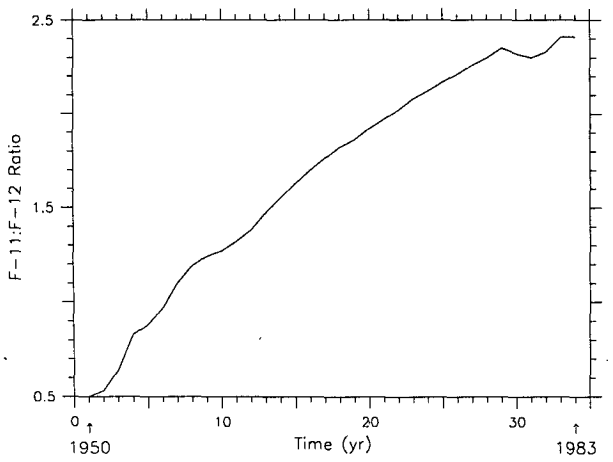

FIG. 1. F-11:F-12 ratio of the surface water, using solubilities (Warner and Weiss 1985) for 0°C, 35‰.

DWBC between 69° and 55°W four times, during which CFM measurements were made. When CFM dating is applied to these sections, a DWBC core speed of only 2 cm s^{-1} is obtained, whereas typical estimates of the DWBC mean speed range from 5 to 15 cm s^{-1} (for example, Worthington 1970; Hogg et al. 1986). This inconsistency suggests that we examine more closely the validity of the CFM dating process, in particular the two assumptions that have been made: 1) that CFM-free mixing occurs in the boundary current, and 2) that the ratio is unaltered in the formation/overflow process.

We present here a simple model of the evolution of CFMs during the deep-water formation and overflow process, and couple this overflow model to two separate boundary current models: the first containing a uniform boundary current, the second a simple sheared current. In each case the deep overflow is the source water for the boundary current. The assumption of CFM-free mixing is relaxed in both boundary current models, as the water adjacent to the boundary current core is allowed to accumulate CFMs. In the overflow model, the sinking surface water resides in the basin for a given amount of time before entering the boundary current. This, along with the mixing in the boundary current, causes the F-11:F-12 ratio to be lowered from its surface value which when applied to the OC134 data set results in increased predictions for the DWBC core speed.

Section 2 contains the overflow basin model and sections 3 and 4 the two boundary current models, with application to the data. A comparison of the boundary current models is contained in section 5 followed by conclusions.

2. Overflow basin model

There are two areas at high latitudes where convective overturning occurs supplying deep water to the northern North Atlantic: the Norwegian–Greenland (N–G) Sea and Labrador Sea. The water which is formed in the N–G Sea is more dense than its Labrador counterpart, and it is this water which upon entrainment forms the DWBC (Worthington 1970). There are three sills over which the newly formed water from the N–G Sea flows into the Atlantic: the Denmark Straits, the Iceland–Faroe Ridge, and Faroe Bank Channel (Fig. 2). The latter two are usually referred to as a single sill called the Iceland–Scotland Ridge.

It is uncertain as to what extent each of these overflows contributes to the water comprising the DWBC. The Iceland–Scotland overflow, shortly after leaving the sill, flows westward through the Gibbs fracture zone. According to Worthington (1970) this current then joins the Denmark Straits overflow and the combined flow progresses southward as the DWBC. Swift (1984) argues that the density of these two overflows is comparable, but that the Iceland–Scotland flow undergoes more intense mixing as it progresses from the sill so that the water which passes through the Gibbs fracture zone is less dense than the Denmark Straits water. As a result, the two currents do not actually combine but rather influence one another. More in line with this, Smethie and Trumbore (1984) present a water property analysis suggesting that the DWBC south of the Grand Banks is comprised mainly of Iceland–Scotland overflow water, and that the Denmark Straits water is found as denser filament-type flows. In this coupled model we assume that the DWBC is composed solely of water of Iceland–Scotland origin; it is clear, however, that there are other elements to be considered and this point should be studied further.

The water which overflows the Iceland–Scotland ridge (as well as that which overflows the Denmark Straits sill) originates from intermediate depths in the overflow basin (Bullister 1984; Swift 1984) and is replenished convectively by surface water which has cooled (Worthington 1970). Only diffusive interaction occurs with the bottom-most basin water. This suggests the following overflow basin model to compute the fluxes of CFMs over the sill. We assume that the surface water, having acquired a CFM concentration according to the atmospheric level at the time, flows into the basin and sinks as a result of heat loss to the atmosphere. This water then resides in the intermediate layer for a while before eventually overflowing. Once below the surface the fluid can mix laterally within the intermediate layer and vertically with the abyssal water.

The input boundary condition for the overflow model is the CFM concentration in the surface Norwegian Sea as a function of time. This was calculated from the atmospheric concentration and the F-11 and F-12 solubility (Warner and Weiss 1985). The equilibration time for CFMs between the surface ocean and the atmosphere is typically ~1 month (Broecker et al. 1980); thus the surface ocean is generally in equilibrium with the atmosphere. In regions of rapid convection however this may not be true, and CFM mea-

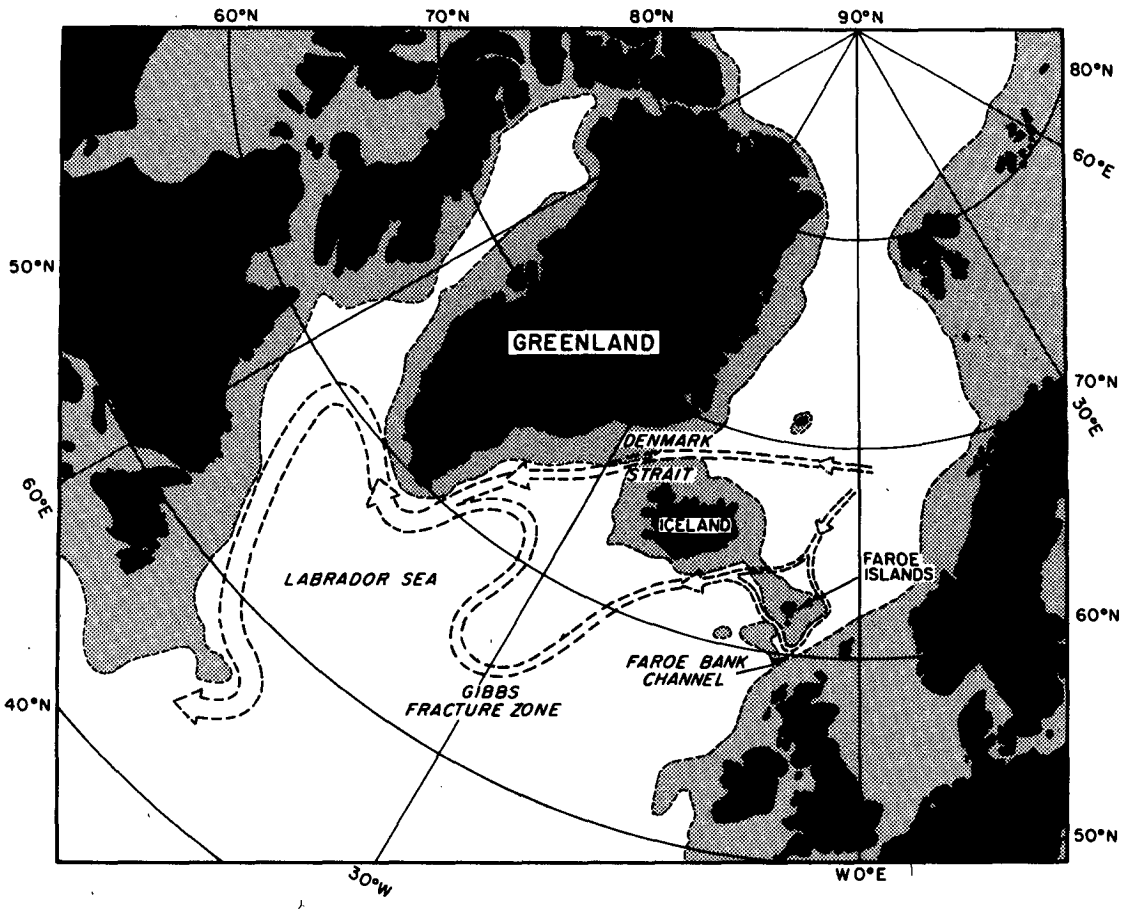

FIG. 2. The three deep overflows of the Norwegian–Greenland Sea (from Warren 1981) which combine to form the DWBC as postulated by Worthington (1970).

surements in the surface Greenland Sea during winter (Bullister and Weiss 1983) have revealed an undersaturation of up to 23 percent. For this simple model, however, we assume equilibrium between the atmosphere and the surface Norwegian Sea.

Figure 3 shows the scenario of the overflow model. In the ocean deep convection occurs as localized events, and because such events can happen throughout the basin we envision a spatially uniform flux from surface layer to intermediate layer which is represented by a specified volume transport of concentration $\theta_i(t)$. We assume as well that the CFMs convected from above are instantaneously diluted throughout the intermediate layer to a uniform concentration $\theta_0(t)$. This type of box model representation has been applied previously to describe the transfer of tracers within the Norwegian–Greenland Sea (e.g., Bullister and Weiss 1983). The concentration of the intermediate layer $\theta_0(t)$ is also the concentration of the overflow, whose transport matches the convective transport. To keep the model as simple as possible we ignore vertical diffusion between the intermediate and abyssal layers.

The CFM budget for the intermediate layer due to this convective source and overflow sink is represented as

$$\frac{d}{dt}F = Q(\theta_i(t) - \theta_0(t)),$$

where F is the total amount of CFMs in the intermediate layer, Q the transport into/out of the intermediate

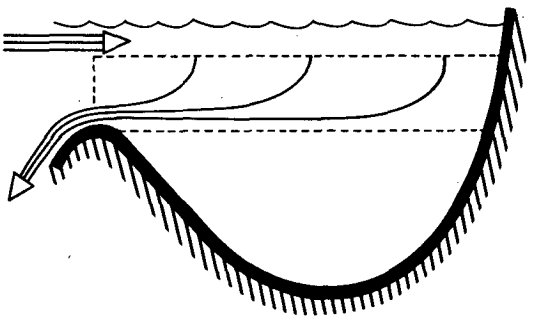

FIG. 3. Simplified scenario of deep water formation and overflow. The dashed region is the intermediate layer whose water comprises the overflow.

layer, $\theta_i(t)$ the surface water concentration, and $\theta_0(t)$ the intermediate layer and overflow concentration. The CFM level F is equal to $V\theta_0(t)$, where V is the volume of the intermediate layer. Constraining V to remain constant the above equation can be rewritten,

$$T_R \frac{d}{dt}\theta_0(t) + \theta_0(t) = \theta_i(t). \quad (1)$$

where $T_R = V/Q$ = residence time of the intermediate layer. Assuming that the intermediate layer is initially free of CFMs, the solution to (1) is

$$\theta_0(t) = \frac{\exp[-(t/T_R)]}{T_R}\int_0^t \exp(t'/T_R)\theta_i(t')dt'. \quad (2)$$

If the residence time of the layer is much less than the time scale of the input, then the overflow concentration is just equal to the surface water concentration as (2) reduces to

$$\theta_0(t) \sim \theta_i(t). \quad (3)$$

In the opposite limit when the input time scale is much smaller than the residence time, (2) simplifies to

$$\theta_0(t) \sim \frac{1}{T_R}\int_0^t \theta_i(t')dt', \quad (4)$$

in which case successive input concentrations are continuously being mixed in the intermediate layer.

Figure 4 shows the surface layer F-12 concentration versus time from 1950 to 1983 (using solubilities for 0°C, 35‰). The sill depth of the Faroe-Bank channel is ~850 m; we assume that the surface layer is 300 m thick and intermediate layer 700 m thick. Transport estimates of the Iceland–Scotland overflow are in the range of 1–2 sverdrups (Worthington 1970; Borenas and Lundberg 1988). Taking the lateral extent of the basin to be 10^6 km^2 this gives a residence time for the intermediate layer of $T_R \sim 10$ years. This value is in

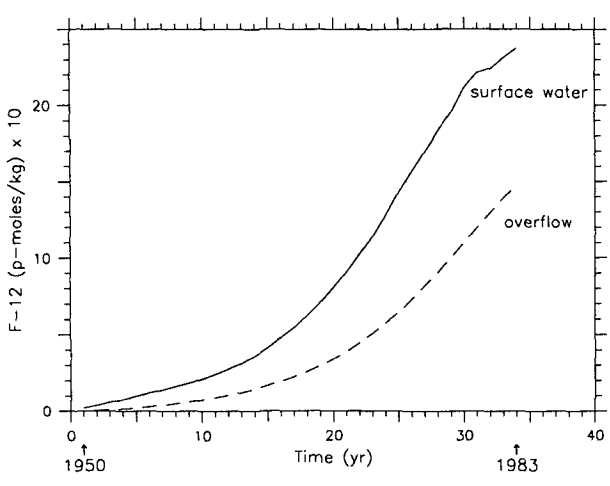

FIG. 4. Concentration of F-12 in the surface water and overflow water, for a basin residence time of 10 yr.

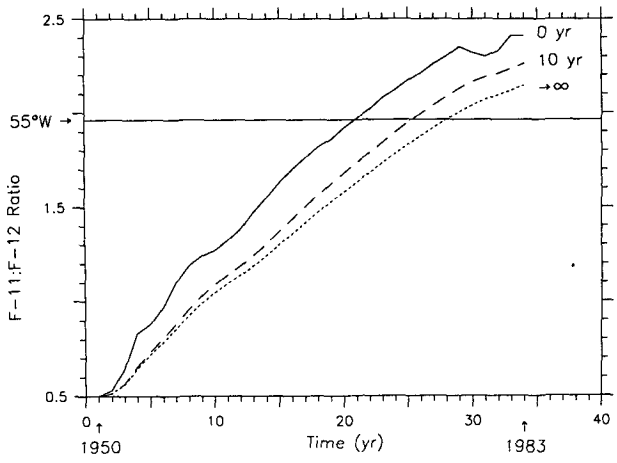

FIG. 5. F-11:F-12 ratio of the overflow water for two different residence times, compared to that of the surface water (T_R = 0 yr). The solid horizontal line is the measured ratio of the DWBC core at 55°W in 1983.

between the limits (3) and (4), and the corresponding F-12 overflow curve is shown in Fig. 4 compared with the surface water concentration curve.

There has been only one cruise which has measured CFMs near the Faroe-Bank channel, RV *Hudson* 82-001 in 1982. Bullister (1984) graphs the values of F-11 and F-12 versus potential density for the two stations nearest the sill. Using an overflow density of $\sigma_2 = 37.37$ (Swift 1984) this gives a F-12 overflow concentration of ~1 p-mol kg^{-1}, which is reasonably close to the model prediction of Fig. 4 for 1982. It should be noted that the agreement could be made perfect by adding a small amount of mixing with a low CFM abyssal layer, and any undersaturation which occurs in the surface layer would also result in slightly reduced overflow concentrations (while leaving the CFM ratio unaltered).

Overflow ratio. We can easily see how the F-11:F-12 ratio is affected by the overflow process. In the small residence time limit the ratio of the overflow is equal to that of the surface water (as are the concentrations themselves). In the large residence time limit (4) gives

$$R_0(t) \sim \int_0^t \theta_{i_1}(t')dt' \Big/ \int_0^t \theta_{i_2}(t')dt', \quad (5)$$

where $R_0(t)$ = ratio of the overflow water and $\theta_{i_1}(t)$, $\theta_{i_2}(t)$ = surface water concentrations of F-11, F-12. In both limits the CFM ratio is independent of the residence time T_R. The corresponding ratio curves are compared in Fig. 5 and the difference between them represents the maximum amount by which the F-11:F-12 ratio can be altered in the overflow basin.

In between these limits the ratio does depend on T_R, and the case for T_R = 10 yr is plotted as well in Fig. 5. Note that because of the mixing which occurs in the

basin the 10-year overflow curve monotonically increases in time in contrast to the surface water curve. This means not only are the ratios lowered, but the ambiguity in determining the age of the water in the boundary current no longer exists. These results suggest that it is important to consider the formation/overflow process when applying CFM dating.

The solid horizontal line in Fig. 5 is the measured F-11:F-12 ratio of the DWBC core at 55°W in 1983, from OC134. Matching this value to the $T_R = 10$ yr overflow curve (assuming CFM-free mixing in the DWBC) gives a transit time of ~8 years over a distance of ~9000 km, which implies an average core speed of ~3.5 cm s^{-1} (when the surface water ratio curve is used in this calculation the predicted core speed is ~2 cm s^{-1}).

3. Uniform boundary current model

The $T_R = 10$ yr overflow curve of the basin model is now used as the upstream boundary condition for a simple model of the DWBC in which the flow is uniform and the CFM concentration is a function of downstream distance only. The important consideration in the model is that the water surrounding the boundary current accumulates CFMs which in turn affect the CFM-ratio of the current.

Initially both the boundary current and surrounding fluid are CFM-free, but as CFMs are first advected from the northern source some diffuse into the surrounding fluid. Then as time progresses and higher CFM ratio water is advected by the current, it mixes with the interior water which has a lower ratio (due to the earlier mixing). This process occurs continuously in time and throughout the length of the boundary current, serving to reduce the ratio of the current.

Both lateral and vertical mixing occur in the boundary current; for simplicity we assume that the resulting fluxes are comparable in strength. Consider the advective-diffusive equation

$$\theta_t + u\theta_x = \kappa\theta_{xx} + \kappa\theta_{yy} + \nu\theta_{zz}. \tag{6}$$

where x, y, z are the alongstream, cross-stream, and vertical coordinates, κ, ν = lateral, vertical eddy diffusivity (assumed constant), u = boundary current velocity, and $\theta(x, y, z, t)$ = CFM concentration. We define H, L_y, and L_x as the vertical, cross-stream, and alongstream length scales of the tracer distribution. It is evident that for the boundary current, $H \ll L_y \ll L_x$. If (6) is scaled accordingly, then the ratio of alongstream diffusion to cross-stream diffusion is $O(L_y/L_x)^2 \ll 1$, and so the dominant balance in (6) is

$$\theta_t + u\theta_x \sim \kappa\theta_{yy} + \nu\theta_{zz}. \tag{7}$$

We now define a stretched vertical coordinate, $z' = (L_y/H)z$, in terms of which (7) becomes

$$\theta_t + u\theta_x \sim \kappa\theta_{yy} + \frac{L_y^2\nu}{H^2}\theta_{z'z'}. \tag{8}$$

Taking $H \sim 1000$ m and $L_y \sim 300$ km as approximate e-folding scales (Fig. 6), this gives $L_y^2/H^2 \sim 10^5$, which means that the lateral and vertical mixing will be comparable in strength if κ and ν are separated by roughly 5 orders of magnitude. We assume this to be the case and set the ratio $\kappa H^2/\nu L_y^2 = 1$. Equation (8) then becomes

$$\theta_t + u\theta_x = \kappa(\theta_{yy} + \theta_{z'z'}), \tag{9}$$

where $\kappa = (L_y^2/H^2)\nu$. This condition means that the vertical diffusive length scale is stretched to the size of the cross-stream diffusive length scale, as diffusion acts isotropically in the y–z' plane. In this coordinate frame the CFM signal of the boundary current appears roughly circular (Fig. 6).

Figure 7 shows a schematic of the deep boundary current (and surrounding fluid) extending from the overflow basin. We define three regions: the core of the current which moves with uniform speed U_c, the adjacent shoulder water (which is motionless), and the "infinite" amount of surrounding fluid. This geometry for the boundary current applies to the stretched coordinate frame defined above. We represent the current

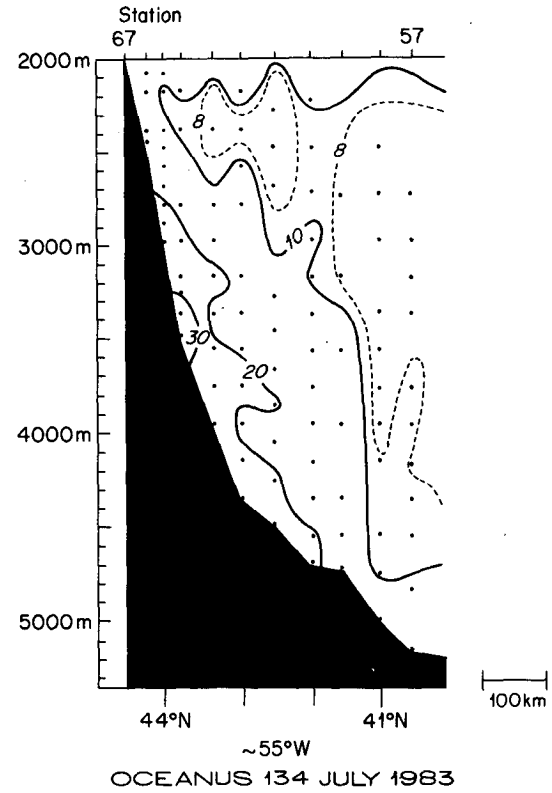

FIG. 6. Vertical section of F-12 (p-mol $kg^{-1} \times 100$ relative to the SIO 1986 scale) below 2000 m, used to estimate the vertical and lateral length scales of the DWBC CFM signal.

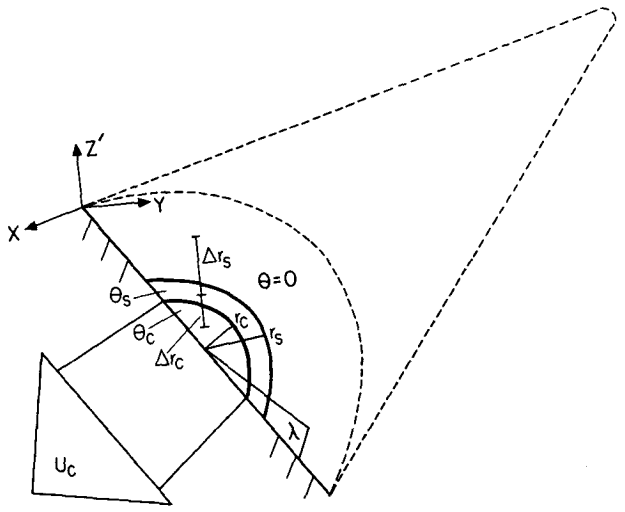

FIG. 7. Schematic of the DWBC showing the core, shoulder, and outer reservoir. The core moves at speed U_c.

using cylindrical coordinates (x, r, λ) where x is the alongstream coordinate, and r and λ are the radial and azimuthal coordinates defined by $y = r\cos\lambda$, $z' = r\sin\lambda$. Equation (9) is thus written

$$\theta_t + u\theta_x = \frac{\kappa}{r}(r\theta_r)_r. \tag{10}$$

In the core region equation (10) is the governing equation with $u = U_c$. The shoulder water acquires tracer by way of diffusion from the core and loses tracer through mixing with the outer reservoir. The shoulder is governed by Eq. (10) with $u \equiv 0$.

Integrating (10) over the cross-sectional area of the core and shoulder regions respectively gives

$$\int_0^{r_c}\int_{\lambda_1}^{\lambda_2} r\theta_t dr d\lambda + U_c\int_0^{r_c}\int_{\lambda_1}^{\lambda_2} r\theta_x dr d\lambda = \kappa\int_{\lambda_1}^{\lambda_2} r\theta_r|_0^{r_c} d\lambda, \tag{11}$$

$$\int_{r_c}^{r_s}\int_{\lambda_1}^{\lambda_2} r\theta_t dr d\lambda = \kappa\int_{\lambda_1}^{\lambda_2} r\theta_r|_{r_c}^{r_s} d\lambda. \tag{12}$$

It is assumed that the concentration of tracer in the boundary current is independent of λ (in the outer reservoir of fluid the concentration is taken to be identically zero). The radial dependency is finite-differenced such that each of the three regions depicted in Fig. 7 is represented by a single concentration. Equations (11) and (12) then become

$$\theta_{c_t} + U_c\theta_{c_x} = (\theta_s - \theta_c)/\tau_c \tag{13}$$

$$\theta_{s_t} = (\theta_c - \gamma\theta_s)/\tau_c \tag{14}$$

where θ_c = core concentration, θ_s = shoulder concentration, and $\gamma = 1 + \tau_c/\tau_s$. The mixing has now been parameterized by two diffusive time scales: $\tau_c = \Delta r_c A/\kappa\pi r_c$ is the mixing time scale between the core and shoulder, and $\tau_s = \Delta r_s A/\kappa\pi r_s$ is the mixing time scale between the shoulder and surrounding reservoir. For simplicity we have taken the cross-sectional area of the core, A, to be equal to that of the shoulder. This assumption also ensures that the shoulder region is not too vast so that it can readily accumulate tracer. The quantities Δr_c and Δr_s are the radial grid spacings (see Fig. 7).

The parameter γ (≥ 1) is called the reservoir parameter; the value of θ_c/γ is the maximum concentration which the shoulder water can attain. In the limit $\tau_s \to 0$ (τ_c finite), $\gamma \to \infty$ and the outer reservoir prohibits any tracer from accumulating in the shoulder region, so the core mixes entirely with CFM-free water. We are thus interested in finite values of γ. When $\tau_s \to \infty$ (τ_c finite), $\gamma \to 1$ and this corresponds to the case when the shoulder water is most readily filled with tracer (the outer reservoir is "turned off"). Thus the larger the value of γ, the more the shoulder water itself acts as a reservoir sink for the core.

To obtain simple analytical solutions to (13) and (14) we approximate the upstream boundary condition overflow curves for F-11 and F-12 by exponentials. The comparisons between the ideal representations and the actual curves are shown in Fig. 8 for the two CFMs and their ratio. While the surface water concentrations have deviated substantially from exponential increase, the deep-water overflows are reasonably represented as such. Using an alongstream finite-difference approach, Pickart (1987) has solved (10) for the actual overflow curves of F-11 and F-12, and the resulting solutions are nearly indistinguishable from those presented below.

The exponential approximation enables (13) and (14) to be solved using separation of variables x and t. The solution for the core concentration is

$$\theta_c(x, t) = \theta_0(t - x/U_c')\exp(-x/U_c'\tau_c') \tag{15}$$

where $\theta_0(t) = A\exp(t/T)$, $U_c' = [1 - 1/(1 + \gamma + \tau_c/T)]U_c$, and $\tau_c' = [(1 + \gamma + \tau_c/T)/(\gamma - 1)]\tau_c$. The time scale T is the e-folding growth time of the deep overflow boundary condition $\theta_0(t)$. For F-11 $T = 7$ yr and for F-12 $T = 8.5$ yr. It is this slight difference which gives rise to CFM dating.

When $\gamma \to \infty$, $U_c' \to U_c$ and $\tau_c' \to \tau_c$, and the solution (15) is that for a uniform boundary current surrounded by a CFM-free basin. In this case, forming the F-11:F-12 ratio using (15) leads to an expression that is easily solved for the core speed,

$$U_c = L\Big/\left(t_0 - \frac{\ln(A_2\phi_1/A_1\phi_2)}{(1/T_1 - 1/T_2)}\right) \tag{16}$$

where L is distance from overflow to measurement (at

55°W); t_0 is time of measurement; ϕ_1, ϕ_2 is F-11, F-12 measurement at 55°W; A_1, A_2 is the amplitude of F-11, F-12 at overflow; and T_1, T_2 the growth time scale of F-11, F-12 at overflow. Using $A_1 = 0.290$ (p-mol kg^{-1} × 10), $A_2 = 0.285$, $T_1 = 7$ yr, $T_2 = 8.5$ yr (Fig. 8), $\phi_1 = 5.87$, $\phi_2 = 2.99$ (values from OC134 in p-mol kg^{-1} × 10 relative to the SIO 1986 scale at the potential temperature of the DWBC core), $t_0 = 34$ yr (=1983), and $L = 8700$ km (distance from the Iceland–Scotland overflow to 55°W from Swift 1984), this gives a DWBC core speed of 3.5 cm s^{-1}.

In the case when the shoulder water is allowed to accumulate CFMs, γ is finite and $U_c' < U_c$, $\tau_c' > \tau_c$, i.e. in the context of (15) the apparent core speed is smaller than the true speed, while the mixing appears weaker. Figure 9 graphs the ratios U_c'/U_c and τ_c/τ_c'. It is seen that for $\gamma \to 1$ the apparent speed is about one-half the true speed.

In the finite γ case, to obtain the value of the core speed the mixing time scale τ_c must be determined as well. By matching the measured values of F-11 and F-12 using (15), this results in the following expressions for U_c and τ_c,

$$U_c = \left[\frac{l_1}{T_1^2} + \frac{l_1(\gamma+1)}{T_1\tau_c} + \frac{l_1(\gamma-1)}{\tau_c^2}\right]\left[\frac{(\tau_c T_1)}{\gamma T_1 + \tau_c)}\right] \tag{17}$$

$$\begin{aligned} 0 = {} & [l_2T_1 - l_1T_2]\tau_c^3 + [(\gamma+1)T_1T_2(l_2 - l_1) \\ & + \gamma(l_2T_1^2 - l_1T_2^2)]\tau_c^2 \\ & + [\gamma(\gamma+1)T_1T_2(l_2T_1 - l_1T_2) \\ & + (\gamma-1)T_1T_2(l_2T_2 - l_1T_1)]\tau_c \\ & + [\gamma(\gamma-1)T_1^2T_2^2(l_2 - l_1)] \end{aligned} \tag{18}$$

where

$$l_i = L \Big/ \left[\ln\left(\frac{\theta_{0_i}(t_0)}{\phi_i}\right)_{i=1,2}\right].$$

For $\gamma > 1$ (18) has one real root which is substituted into (17) to obtain the core speed. Figure 10 plots U_c as a function of the reservoir parameter γ. When $\gamma \to \infty$ (17) gives a value of $U_c = 3.5$ cm s^{-1} [as does (16)], and as γ gets smaller the core speed increases. When γ is identically equal to one the real root of (18) is

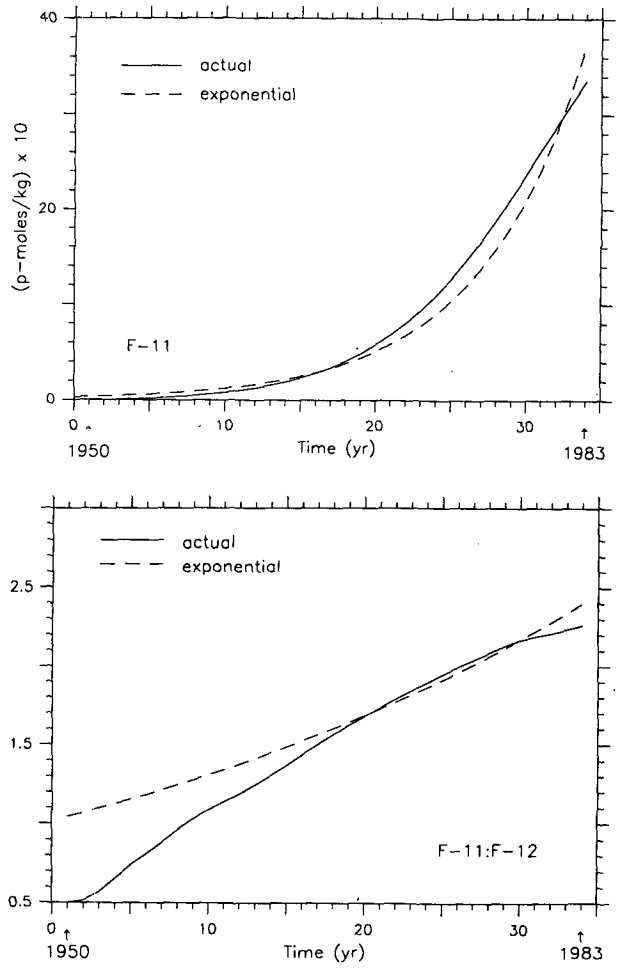

FIG. 8. (a) $T_R = 10$ yr overflow concentration of F-11 from the model (solid line) compared to the exponential approximation $A \exp(t/T)$ (dashed line), with $A = 0.290$ p-mol kg^{-1} × 10, $T = 7$ yr. (b) Same comparison for F-12, with $A = 0.285$ p-mol kg^{-1} × 10, $T = 8.5$ yr. (c) Comparison of the F-11:F-12 ratio.

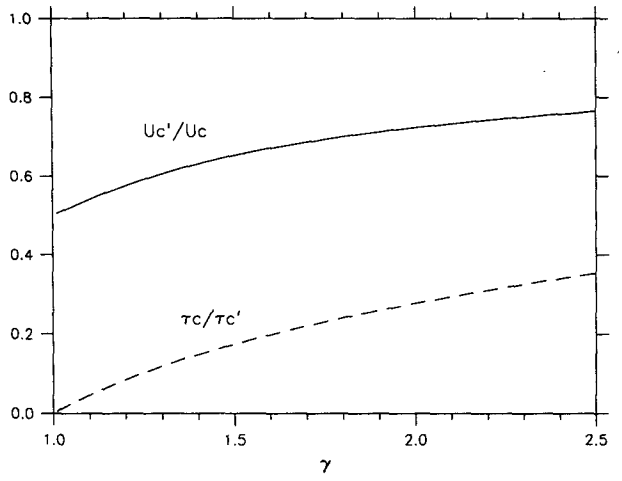

FIG. 9. Ratio of the true and apparent core speed and mixing time scale.

$\tau_c = 0$ (consistent with the definition of γ). In this case the shoulder water accumulates such a large amount of CFMs that in order for it to dilute the core the time scale of mixing between the core and shoulder must be infinitely short. From (17) $U_c \to 6.9$ cm s^{-1} when $\gamma \to 1$ and $\tau_c \to 0$ (Fig. 10).

One of the observations that has led to the assumption of CFM-free mixing in the deep basins is the weak alongstream variation of the CFM ratio in deep currents (Smethie and Trumbore 1984). Because the ratio is not a conserved quantity in this model (for finite γ) it might seem that the resulting downstream variation contradicts this observation. It is the case, however, that while U_c and τ_c are strongly dependent on γ, U_c' and τ_c' depend only weakly on γ, i.e. the apparent speed and apparent mixing are nearly equal to the CFM-free values of core speed and mixing. This in turn means that the CFM core concentration (15) is itself nearly independent of γ. Figure 11 shows good agreement between the predicted F-12 concentration and F-11: F-12 ratio and the values measured during OC134 between 55° and 69°W.

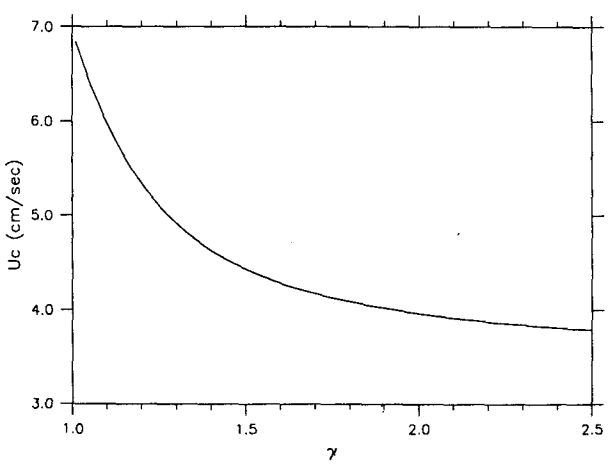

FIG. 10. DWBC core speed as a function of the reservoir parameter γ.

4. Boundary current with cross-stream shear

In the previous model the DWBC was represented as a single core velocity, and it was seen that mixing between the core and adjacent shoulder water resulted in decay of the core ratio when the shoulder did not act as an infinite sink of CFMs. In this section we consider a deep boundary current with cross-stream shear, and assume that the core of the current mixes entirely with the outlying weaker flow. Because the slower moving water is older (and has a lower CFM ratio) this tends to decrease the core ratio.

As before the boundary current is comprised of a core and shoulder, adjacent to a vast amount of surrounding fluid (which again is taken to be an infinite sink of CFMs, Fig. 12). The difference in this model is that the shoulder water is moving as well: the core moves at speed U_c, the shoulder at speed U_s ($<U_c$). We assume as before that the concentrations are uniform in the azimuthal direction, and apply the same radial finite-difference approximation.

The governing equation is again (10), with $u = U_c$ in the core, $u = U_s$ in the shoulder. In this model we take $r_c \ll r_s$ (Fig. 12) which means that the surface area of contact between the core and shoulder is so small that the diffusive flux of CFMs into the shoulder across this surface is negligible compared with the flux across the outer surface of the shoulder. Note then that the mechanism by which the shoulder accumulated CFMs in the uniform current model is absent in this model; rather the shoulder receives CFMs advectively from the overflow.

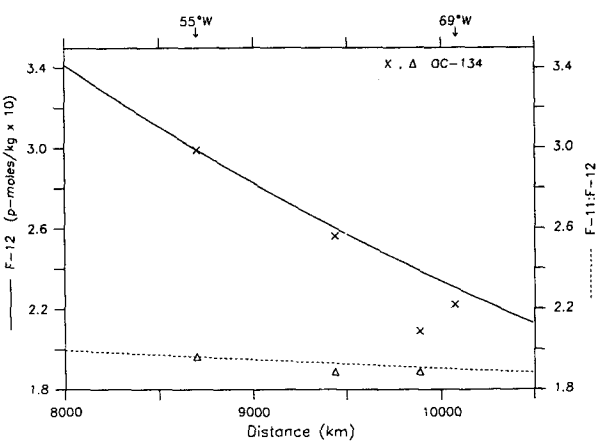

FIG. 11. Alongstream variation in core concentration and ratio as predicted by the model (solid and dashed curves respectively), compared to the values measured during OC134. The model solution has been matched to the data at 55°W, and is nearly independent of the value of γ chosen as explained in the text.

Integrating (10) over the core and shoulder cross-sections as before, and applying the radial finite-difference approximation results in the following set of equations [to be compared with (13) and (14)],

$$\theta_{c_t} + U_c\theta_{c_x} = (\theta_s - \theta_c)/\tau_c \tag{19}$$

$$\theta_{s_t} + U_s\theta_{s_x} = -\theta_s/\tau_s \tag{20}$$

where τ_c and τ_s are defined as before. Since we have introduced another unknown, U_s, we must also introduce another parameter. In the previous model we expressed solutions in terms of the reservoir parameter $\gamma = 1 + \tau_c/\tau_s$, which includes the ratio of the mixing coefficients. Here we also form the ratio of the velocities, U_c/U_s, which is taken to be greater than or equal to one.

As before the deep overflow boundary condition is approximated by an exponential, $A\exp(t/T)$, and solutions are obtained by separation of variables. The expression for the core concentration is

$$\theta_c(x, t) = A\exp(t/T)\left[\exp\left[-\left(\frac{1}{T}+\frac{1}{\tau_c}\right)\frac{x}{U_c}\right] + \frac{\exp\left[-\left(\frac{U_c}{U_s}\left(\frac{1}{T}+\frac{(\gamma-1)}{\tau_c}\right)\frac{x}{U_c}\right]\right] - \exp\left[-\left(\frac{1}{T}+\frac{1}{\tau_c}\right)\frac{x}{U_c}\right]}{\left(\frac{\tau_c}{T}+1\right) - \frac{U_c}{U_s}\left(\frac{\tau_c}{T}+\gamma-1\right)}\right]. \tag{21}$$

By matching (21) to the measured values of F-11 and F-12 at 55°W, one obtains a coupled set of nonlinear equations for U_c and τ_c, which in turn can be solved using a numerical fixed point iterative method. For a reasonably close initial estimate, convergence to the fixed point (U_c, τ_c) occurs within the first several iterations.

Figure 13 plots the core speed versus the ratio U_c/U_s, for three different values of the reservoir parameter γ. A smaller value of γ means the shoulder water is diluted more slowly by the surrounding reservoir, which means there is a higher concentration of CFMs in the shoulder by which to lower the core ratio through mixing. This in turn gives an increased value of the core speed. When the shoulder speed is equal to that of the core ($U_c/U_s = 1$), the F-11:F-12 ratio of the shoulder is the same as the core ratio (although the concentrations themselves are lower). This is analogous to the uniform boundary current case of mixing with a CFM-free reservoir, and the resulting core speed is the CFM-free value of 3.5 cm s^{-1}. In the other extreme, $U_c/U_s \to \infty$ (infinite lag between the core and shoulder), the shoulder receives no CFMs from the source and again the core speed is 3.5 cm s^{-1}. In between these limits the core speed reaches a maximum for a given value of U_c/U_s depending on the value of γ. In Fig. 13 the $\gamma = 1.03$ curve is continually increasing, while the $\gamma = 1.25$ curve obtains its maximum and then starts to asymptote to the CFM-free core speed.

While U_c is a strong function of the ratio U_c/U_s, the shoulder speed, U_s, remains in the 2–3 cm s^{-1} range regardless of the size of U_c/U_s or γ. This is not surprising, for the shoulder mixes exclusively with the CFM-free surrounding water (recall that the flux of CFMs from core to shoulder is negligible). This puts an upper limit on U_s equal to the CFM-free value of 3.5 cm s^{-1}. The core concentration (21) is also only weakly dependent on U_c/U_s and γ, and as was the case in the uniform boundary current, the predicted alongstream variation in F-12 and F-11:F-12 ratio is in good agreement with the data.

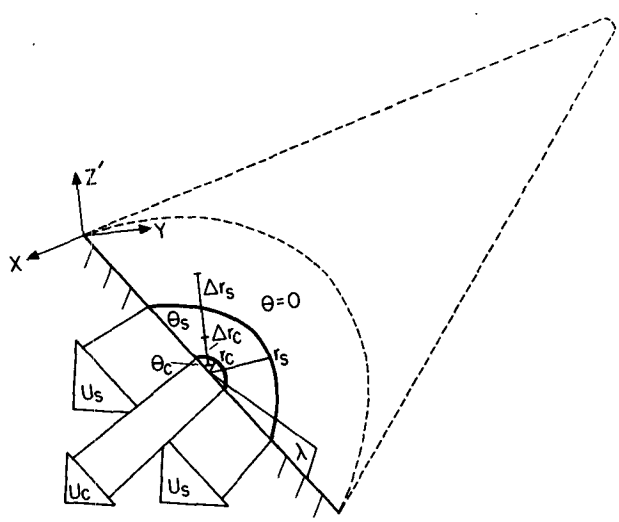

FIG. 12. The DWBC as represented in Fig. 7, only with flow in both the core and shoulder regions.

5. Comparison of the boundary currents

In both of the boundary current models there is a range of possible solutions, each with a different value of the core speed and mixing coefficient. We now compare a given solution from each model and relate them to what is known about the DWBC and its associated CFM signal. This helps to clarify the distinguishing features of the two models.

We do not wish to consider solutions with a small (<4 cm s^{-1}) core speed as such a value is not representative of the DWBC. We also do not use the max-

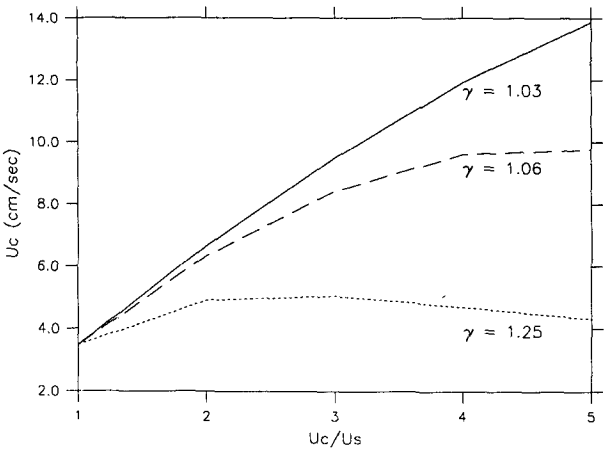

FIG. 13. DWBC core speed versus the ratio U_c/U_s, for three different values of the reservoir parameter γ.

imum core speed solutions in either of the models, for the following reasons. In the uniform boundary current, as $\gamma \rightarrow 1$, the cross-stream variation in CFMs (between the core and shoulder) vanishes. As the ratio $U_c/U_s \rightarrow \infty$ in the sheared boundary current, the opposite occurs as the concentration of the shoulder water goes to zero. These features are unacceptable, and in fact, there is only a small range of solutions for each model which are physically plausible.

We compare the 5 cm s^{-1} solution for the uniform current, and the 10 cm s^{-1} ($\gamma = 1.03$) solution for the boundary current with cross-stream shear. In each model we are free to specify the value of r_s, the width of the CFM signal. In the uniform flow r_c is then known because the core and shoulder cross-sectional areas are the same (Fig. 7), and in the sheared flow r_c must satisfy the relation $r_c \ll r_s$ (Fig. 12).

When written in terms of the radial distances, the mixing time scale τ_c (which is known from the matching) takes the form $\tau_c = r_c r_s/4\kappa$, where κ is the lateral diffusivity. It is evident that in specifying the width r_s (and therefore r_c) this will determine both the transport of the current and the value of the diffusivity. Figure 14 plots the transport versus κ for different values of the width (recall that the vertical diffusivity ν is related to κ by (9)). Both models predict comparable transports, however the resulting cross-stream variation in CFM concentration is closest to that observed in the data for small transports [$\sim$5 Sv (Sv $\equiv 10^6$ m^3 s^{-1})] for the uniform current, and large transports ($\sim$15 Sv) for the sheared current.

We can now more fully appreciate the differences between the two boundary current models. The uniform boundary current has limited cross-stream extent and a small transport; high concentrations of CFMs are found in the water surrounding the flow. The sheared boundary current is much broader with more intense flow at the core, and has a large transport. Only a small amount of CFMs accumulate in the water adjacent to the current. These differences are depicted in Fig. 15.

There is some uncertainty as to what constitutes an average value of the DWBC core speed, as well as its transport. The DWBC is known to pulsate in time (Richardson 1977) as well as meander up and down the continental slope (Luyten 1977), both of which make it difficult to determine these quantities. Transport estimates vary from as small as 4 Sv (Pierce 1986) to as large as 24 Sv (Richardson 1977), although the former is a synoptic estimate and the latter includes water as shallow as 200 m. Most estimates are in the range of 8–12 Sv (for example, Joyce et al. 1986; Hogg 1983; Richardson and Knauss 1971). Numerous direct measurements of the DWBC core speed have been made. Instantaneous values as large as 45 cm s^{-1} have been reported (Richardson 1977), although mean speeds appear to be in the range of 5–8 cm s^{-1} (Luyten 1977; Richardson 1977). Both of the boundary current solutions compared above fall within this range of transports and core speeds.

6. Summary

Two simple advective–diffusive boundary current models have been presented to show how mixing can reduce the F-11:F-12 ratio in the core of the DWBC. When coupled to a convection model of the Iceland–Scotland overflow (whose output is the northern boundary condition for the current), core speeds of 5–10 cm s^{-1} are predicted for the DWBC from matching model solutions to CFM data collected along the western boundary. This is in contrast to a core speed of only 2 cm s^{-1} which is obtained when one assumes that CFM-free mixing occurs in the current and that the CFM ratio is not altered during deep water for-

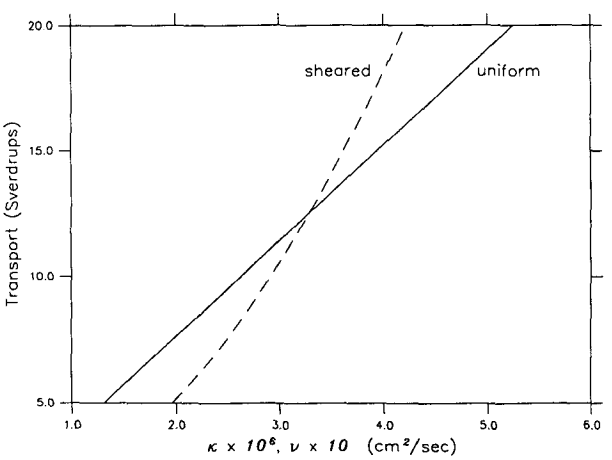

FIG. 14. DWBC transport versus diffusivity for the two boundary currents.

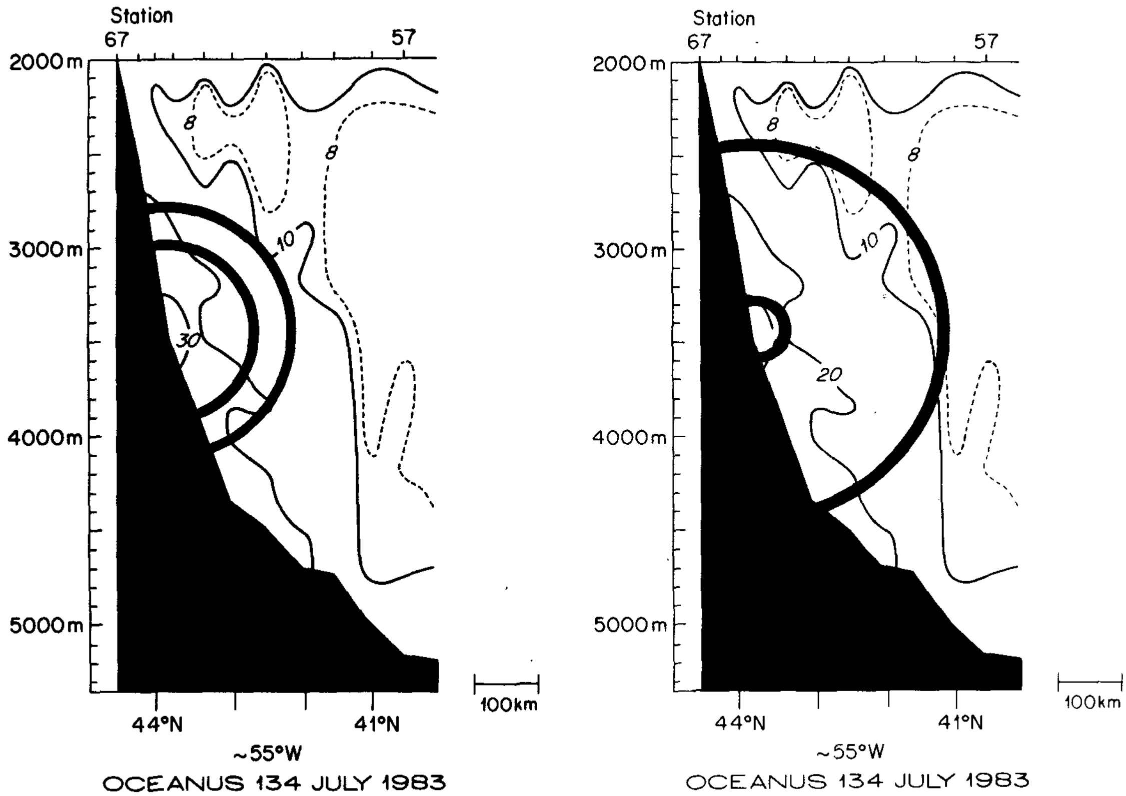

FIG. 15. (a) The core and shoulder regions (denoted by thick lines) of the 5 Sv solution for the uniform boundary current, superimposed on the DWBC F-12 signal of Fig. 6. (b) The 15 Sv solution for the sheared boundary current.

mation and overflow (when only the first assumption is made and the overflow model is applied alone, the predicted core speed is 3.5 cm s^{-1}).

When the DWBC is modeled as a uniform flow, its CFM ratio is altered through mixing with surrounding water which diffusively accumulates CFMs from the current. The most realistic solution gives a transport of ~5 Sv. When the boundary current contains cross-stream shear, its core ratio decays due to mixing with the slower outlying flow. In this case a transport of ~15 Sv is predicted. Both solutions give values of $O(10^6)$ cm^2 s^{-1} for lateral diffusivity, $O(10)$ cm^2 s^{-1} for vertical diffusivity. Although neither of the models is entirely satisfactory by itself, they do suggest that to some extent both ratio decay mechanisms may be present in the DWBC.

Acknowledgments. The authors wish to acknowledge the help of Susan Trumbore in collecting and processing the CFM data. R.P. and N.H. were supported by the Office of Naval Research through Contracts N00014-76-C-0197 and N00014-84-C-0132, NR 083-400; and N00014-82-C-0019 and N00014-85-C-0001, NR 083-004, and the National Science Foundation through Grant OCE82-14925. W.S. was supported by the National Science Foundation through Grant OCE83-00031.

REFERENCES

Borenas, K. M., and P. A. Lundberg, 1988: On deep water flow through the Faroe Bank Channel. *J. Geophys. Res.*, **93**, 1281–1292.

Broecker, W. S., T.-H. Peng and T. Takahashi, 1980: A strategy for the use of bomb-produced radiocarbon as a tracer for the transport of fossil fuel CO_2 into the deep-sea source regions. *Earth Planet. Sci. Lett.*, **49**, 463–468.

Bullister, J. L., 1984: Atmospheric Chlorofluoromethanes as tracers of ocean circulation and mixing: measurement and calibration techniques and studies in the Greenland and Norwegian Seas. Ph.D. thesis, University of California, San Diego.

——, and R. F. Weiss, 1983: Anthropogenic chlorofluoromethanes in the Greenland and Norwegian seas. *Science*, **221**, 265–268.

Chemical Manufacturers Association, 1983: CMA CFC-11 and CFC-12 production and release data, 14 pp.

Cunnold, D. M., R. G. Prinn, R. A. Rasmussen, P. G. Simmonds, F. N. Alyea, C. A. Cardelino, A. J. Crawford, P. J. Fraser and R. D. Rosen, 1983a: The atmospheric lifetime experiment, IV: Lifetime methodology and application to three years of $CFCl_3$ data. *J. Geophys. Res.*, **88**, 8379–8400.

——, ——, ——, ——, ——, ——, ——, —— and ——, 1983b: The atmospheric lifetime experiment, V: Results for CF_2Cl_2 based on three years data. *J. Geophys. Res.*, **88**, 8401–8414.

——, ——, ——, ——, ——, ——, ——, —— and ——, 1986: Atmospheric lifetime and annual release estimates for $CFCl_3$ and CF_2Cl_2 from 5 years of ALE data. *J. Geophys. Res.*, **91**, 10 797–10 817.

Fine, R. A., and R. L. Molinari, 1988: A continuous deep western boundary current between Abaco (26.5°N) and Barbados (13°N). *Deep-Sea Res.*, **35**, 1441–1450.

Gammon, R. H., and J. Bullister, 1982: Freon penetration into the North Atlantic deep water. *Trans. Amer. Geophys. Union,* **63,** 77.

Hogg, N. G., 1983: A note on the deep circulation of the western North Atlantic: its nature and causes. *Deep-Sea Res.,* **30,** 945–961.

——, R. S. Pickart, R. M. Hendry and W. M. Smethie Jr., 1986: The northern recirculation gyre of the Gulf Stream. *Deep-Sea Res.,* **33,** 1139–1165.

Joyce, T. M., C. Wunsch and S. D. Pierce, 1986: Synoptic Gulf Stream velocity profiles through simultaneous inversion of hydrographic and acoustic Doppler data. *J. Geophys. Res.,* **91,** 7573–7585.

Luyten, J. R., 1977: Scales of motion in the Deep Gulf Stream and across the continental rise. *J. Mar. Res.,* **35,** 49–74.

McCarthy, R. L., F. A. Bower and J. P. Jesson, 1977: Production and release of CCl_3F and CCl_2F_2 (Fluorocarbons 11 and 12) through 1975. *Atmos. Environ.,* **11,** 491–497.

Pickart, R. S., 1987: The entrainment and homogenization of tracers within the cyclonic Gulf Stream recirculation gyre. Ph.D. thesis, Massachusetts Institute of Technology and Woods Hole Oceanographic Institution, Woods Hole, MA, 210 pp.

Pierce, S. D., 1986: Gulf Stream velocity structure through combined inversion of hydrographic and acoustic doppler data. M.S. thesis, Dept. of Earth, Atmospheric, and Planetary Sciences, Massachusetts Institute of Technology, 65 pp.

Rasmussen, R. A., M. A. K. Khalik and R. W. Dalluge, 1981: Atmospheric trace gases in Antarctica. *Science,* **211,** 285–287.

Richardson, P. L., 1977: On the crossover between the Gulf Stream and the western boundary undercurrent. *Deep-Sea Res.,* **24,** 139–159.

——, and J. A. Knauss, 1971: Gulf Stream and western boundary undercurrent observations at Cape Hatteras. *Deep-Sea Res.,* **18,** 1089–1109.

Smethie, W. M. Jr., and S. Trumbore, 1984: Chlorofluoromethanes (F-11 and F-12) in the western North Atlantic Ocean and the deep western boundary undercurrent. *Eos, Trans. Amer. Geophys. Union,* **64,** p. 1089.

——, D. W. Chipman, J. H. Swift and K. P. Koltermann, 1988: Chlorofluoromethanes in the Arctic Mediterranean seas: evidence for formation of bottom water in the Eurasian basin and deep-water exchange through Fram strait. *Deep-Sea Res.,* **35,** 347–369.

Swift, J. H., 1984: The circulation of the Denmark Strait and Iceland-Scotland overflow waters in the North Atlantic. *Deep-Sea Res.,* **31,** 1339–1355.

Warner, M. J., and R. F. Weiss, 1985: Solubilities of chlorofluorocarbons 11 and 12 in water and seawater. *Deep-Sea Res.,* **32,** 1485–1497.

Warren, B. A., 1981: Deep circulation of the world ocean. *Evolution of Physical Oceanography,* B. A. Warren and C. Wunsch, Eds., The MIT Press, 6–41.

Weiss, R. F., J. L. Bullister, R. H. Gammon and M. J. Warner, 1985: Atmospheric chlorofluoromethanes in the deep equatorial Atlantic. *Nature,* **314,** 608–610.

Worthington, L. V., 1970: The Norwegian Sea as a Mediterranean basin. *Deep-Sea Res.,* **17,** 77–84.